Environmental Science & Technology

pubs.acs.org/est

Article

Coprecipitation of Phosphate and Silicate Affects Environmental Iron (Oxyhydr)Oxide Transformations: A Gel-Based Diffusive Sampler Approach

Peter Kraal,* Case M. van Genuchten, Wytze K. Lenstra, and Thilo Behrends

Cite This: *Environ. Sci. Technol.* 2020, 54, 12795−12802

Read Online

ABSTRACT: Sorption of nutrients such as phosphate (P) and silicate (Si) by ferric iron (oxyhydr)oxides (FeOx) modulates nutrient mobility and alters the structure and reactivity of the FeOx. We investigated the impact of these interactions on FeOx transformations using a novel approach with samplers containing synthetic FeOx embedded in diffusive hydrogels. The FeOx were prepared by Fe(III) hydrolysis and Fe(II) oxidation, in the absence and presence of P or Si. Coprecipitation of P or Si during synthesis altered the structure of Fe precipitates and, in the case of Fe(II) oxidation, lepidocrocite was (partly) substituted by poorly ordered FeOx. The pure and P- or Si-bearing FeOx were deployed in (i) freshwater sediment rich in dissolved Fe(II) and P and (ii) marine sediment with sulfidic pore water. Iron(II)-catalyzed crystallization of poorly ordered FeOx was negligible, likely due to surface passivation by adsorption of dissolved P. Reaction with dissolved sulfide was modulated by diffusion limitations and therefore the extent of sulfidation was the lowest for poorly ordered FeOx with high reactivity toward sulfide that created temporary, local sulfide depletion (Fh < Lp). We show that coprecipitation-induced changes in the FeOx structure affect coupled iron-nutrient cycling in aquatic ecosystems. The gel-based method enriches our geochemical toolbox by enabling detailed characterization of target phases under natural conditions.

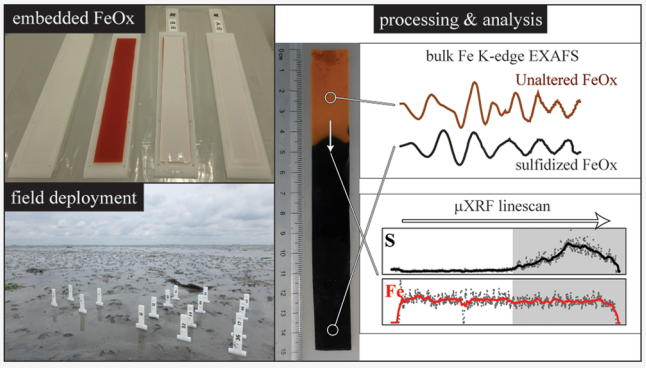

INTRODUCTION

Poorly crystalline ferric iron (oxyhydr)oxides (FeOx) have high sorption capacity and therefore modulate the mobility and bioavailability of (trace) contaminants and nutrients in aquatic systems. Furthermore, laboratory studies have shown that adsorption or coprecipitation of such species can alter the transformation and dissolution of FeOx such as ferrihydrite (Fh) and lepidocrocite (Lp). Strong effects have been observed in laboratory studies for nutrients such as phosphate (PO_4, denoted here as P) and silicate (SiO_4, denoted here as Si).[1−6]

Occupation of FeOx surface sites by oxyanions such as PO_4 or SiO_4 during Fe precipitate formation decreases structural order. The extent of the impact depends on the molar oxyanion/Fe ratio and the FeOx-formation pathway. Sorption of oxyanions during Fe(III) hydrolysis and Fe(II) oxidation disrupts Fe−Fe polymerization and under high oxyanion/Fe ratios, amorphous precipitates such as Fe(III) phosphate can form.[7,8] Furthermore, in the case of Fe(II) oxidation, sorption of oxyanions inhibits Fe(II)-catalyzed transformation of freshly formed nanoscale FeOx into more crystalline Fe phases.[3,7−10] The environmental implications of these FeOx alterations are poorly known. In particular, it is unclear how key FeOx transformation pathways such as crystallization and sulfidation are affected under natural conditions. These transformations alter the nutrient and contaminant sorption capacities of Fe minerals and represent key processes in the coupling between nutrient dynamics and Fe redox cycling and transformation.[11−13]

Detailed tracking of the environmental fate of target Fe phases can be complicated by interference from a large and diverse pool of background Fe in natural sediments. Laboratory-based batch and column experiments[14−18] have provided detailed insight into FeOx transformations but may not adequately represent natural conditions, in part because of the use of FeOx as a single solid phase or synthetic sediment. Here, we aim to advance our understanding of the environmental fate of Fe by adapting an established pore-water method (diffusive gradients/equilibrium in thin films, DGT−DET)[19,20] to deploy well-characterized (P-bearing) FeOx, embedded in diffusive hydrogels, in natural sediments. We

Received: April 15, 2020
Revised: September 2, 2020
Accepted: September 4, 2020
Published: September 4, 2020

https://dx.doi.org/10.1021/acs.est.0c02352
Environ. Sci. Technol. 2020, 54, 12795−12802

show that the target FeOx undergo geochemical transformations (with a prominent role for P and Si coprecipitation) that can be investigated in (microscale) detail because the hydrogels only contain FeOx and its transformation products.

■ MATERIALS AND METHODS

Synthesis of Iron Precipitates. Two-line ferrihydrite (Fh; $Fe(III)_{10}O_{14}(OH)_2 \cdot nH_2O$ with $n < 1$)[21,22] and lepidocrocite (Lp; γ-Fe(III)OOH), referred to here as "pure" FeOx, were prepared following established protocols using Fe(III) hydrolysis for Fh synthesis and Fe(II) oxidation for Lp synthesis at circumneutral pH (7−8).[23] Base hydrolysis of a concentrated Fe(III) solution is a widely used method to synthesize Fh-type precipitates representative of poorly ordered FeOx in natural soils and sediments. Such precipitates form in anthropogenic landscapes by neutralization of acidic, Fe(III)-rich drainage from acid sulfate soils and mine tailings, where the FeOx play an important role in scavenging contaminants.[24−27] Lepidocrocite from oxidation of a concentrated Fe(II) solution serves as an analogue for more crystalline natural FeOx formed around redox interfaces in natural soils and sediments where initial poorly ordered FeOx precipitates undergo further crystallization by reaction with Fe(II).[13,28,29]

In addition to pure FeOx, we prepared FeOx with coprecipitated P or Si at a molar (P, Si)/Fe ratio of 0.1. A P/Fe ratio of 0.1 is representative of the ratio between Fe(III) and associated P in oxic surface sediments.[30−32] Furthermore, previous studies have elucidated in detail the impact of P and Si coprecipitation on the FeOx structure at similar oxyanion/Fe ratios.[3,7,10] The FeOx prepared by Fe(III) hydrolysis and Fe(II) oxidation are referred to as $FeOx_{hydr}$ and $FeOx_{oxid}$, respectively. Details of FeOx synthesis are given in the Supporting Information and have been reported previously.[6]

Preparation of (FeOx-Bearing) Hydrogels and Samplers. Several types of (bis)acrylamide-cross-linked hydrogels were prepared. Using existing protocols, DET (diffusive equilibrium in thin films[19]) hydrogels were prepared for measurement of pore-water Fe(II)[33] and P[34] and DGT (diffusive gradients in thin films)-binding hydrogels were prepared for pore-water sulfide.[35] Using an adapted protocol (see the Supporting Information), FeOx-bearing thin-film (FeOx-BT) hydrogels were prepared by adding small aliquots of FeOx in suspension during hydrogel casting. Diffusive samplers for pore-water analysis or FeOx deployment were prepared by placing DGT−DET or FeOx-BT hydrogels, covered with a filter membrane, in rigid Teflon samplers (DGT Research, Lancaster) as detailed in the Supporting Information. The FeOx-BT samplers allow diffusive exchange with pore water but prevent direct physical contact between the target FeOx and solid-phase sediment (i.e., contamination).

Deployment of Hydrogel Samplers. Samplers were deployed during the summer period (June−September) of 2016 at two contrasting sites in The Netherlands. Site 1 was a freshwater drainage ditch on the Utrecht University campus (52°5.27′ N, 5°9.80′ E) with clayey to sandy sediment rich in dissolved Fe(II) and P. Site 2 was a tidal mud flat with sulfidic silty to sandy sediment in the marine Oosterschelde estuary (salinity 28 PSU) in the southwest of The Netherlands (51°26.35′ N, 4°9.87′ E). Site 1 was used to investigate Fe(II)-catalyzed transformation of Fh and Site 2 was used to study Fh and Lp sulfidation. At each site, DGT−DET and FeOx-BT samplers were introduced into the sediment. Pore-water samplers were left overnight; the FeOx were deployed for four weeks. Details on the deployment and recovery of the samplers are given in the Supporting Information. We conducted an additional short-term FeOx sulfidation experiment under controlled conditions. For this laboratory-based experiment, a microcosm of surface sediment with 5 cm of overlying water was created using mixed surface sediment (top 10 cm) and unfiltered seawater from Site 2. These benthic microcosms were left to equilibrate at room temperature for a week while the overlying water was kept O_2-saturated by bubbling air through it. Subsequently, pore-water samplers and FeOx-BT samplers were inserted and left overnight.

In the field and laboratory experiments, the DGT−DET pore-water samplers were deployed in sets of two to measure $\sum H_2S$ (DGT) and Fe (DET) or $\sum H_2S$ (DGT) and P (DET). During the field experiments, we deployed duplicate samplers for each type of FeOx-BT hydrogel. In the laboratory sulfidation experiment, single samplers for each type of FeOx-BT hydrogel were used.

Processing of DET−DGT and FeOx-BT Hydrogels. The pore-water DGT and DET hydrogels were analyzed as described previously (also see the Supporting Information). Briefly, DET hydrogels that had equilibrated with pore water were overlain with a DET hydrogel that had equilibrated with a solution containing reagent for spectrophotometric detection of either Fe(II) (ferrozine) or P (molybdate blue). Color formation by diffusive exchange between the sample and staining gels was quantified and converted into dissolved Fe(II) or P concentration.[33,34] In DGT gels, sulfide is bound as black-colored Ag_2S, which stains the initially white gel. From the intensity of this color change, the dissolved sulfide concentration can be calculated.[35]

The FeOx-BT hydrogels were removed from the samplers in an Ar-filled anoxic glovebox. One of the duplicate gels was immediately cut horizontally into four equal pieces of ∼3.5 cm length and 1.5 cm width. These gel cuts were shortly stored in anoxic milliQ (with two water changes to remove any dissolved components) prior to further preparation for X-ray analysis. The second duplicate gel was stored intact in Ar-purged anoxic milliQ. A selection of these duplicate gels (Fh, P9-$FeOx_{hydr}$, Si9-$FeOx_{hydr}$) was cut as described above and used for microscale X-ray fluorescence (μXRF) scanning.

Microscale XRF and Synchrotron-Based X-Ray Absorption Spectroscopy (XAS) Analysis of Hydrogel Sections. Detailed descriptions of sample preparation and analysis for μXRF and XAS analyses are given in the Supporting Information. Briefly, for the μXRF analysis, selected duplicate wet gel cuts were placed on microscope slides and vertical line scans were collected at 30 μm resolution for Fe, P, and S. For synchrotron-based X-ray absorption spectroscopy (XAS), samples were freeze-dried, ground, and mixed with cellulose and pressed into pellets that were used for Fe K-edge XAS analysis at beamline BM26A (DUBBLE) of the European Synchrotron Radiation Facility (ESRF) in Grenoble, France. Details on the beamline setup can be found in Nikitenko et al.[36] Spectra were recorded at room temperature in transmission mode from 6962 to 7862 eV, corresponding to a maximum k of 13 $Å^{-1}$ in the extended X-ray absorption fine structure (EXAFS) region. For each sample, two spectra were collected and merged. Repeated measurement of an FeS-rich sample showed no sign of oxidation or beam damage during

https://dx.doi.org/10.1021/acs.est.0c02352
Environ. Sci. Technol. 2020, 54, 12795−12802

analysis. Data normalization was done using the Athena software package.[37] Iron speciation was obtained by linear combination fitting of components (representing Fe phases) extracted from the entire XAS data set (24 spectra including references) by iterative transform factor analysis using the ITFA software package.[38] Analysis was performed in the k space, using a fitting window of k = 2−11 Å^{-1} of the k^3-weighted EXAFS spectra. For sulfidation samples, the degree of Fe sulfidation (DOS)[39] was determined as the fraction of total Fe transformed into iron (mono)sulfide based on the results from the LCF.

■ RESULTS AND DISCUSSION

Structure of the Initial FeOx. Hydrolysis of concentrated Fe(III) solutions formed Fh-type precipitates (Figure 1).

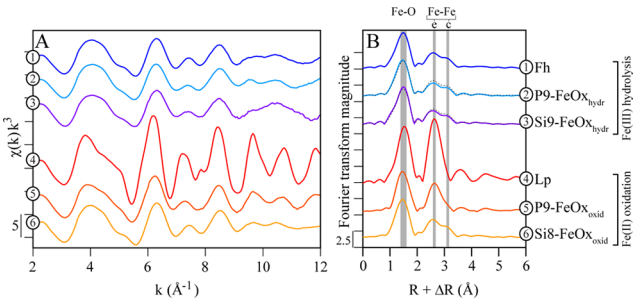

Figure 1. (A) Fe K-edge EXAFS spectra and (B) Fourier-transformed Fe K-edge EXAFS spectra of FeOx synthesized for this study. Vertical gray bands in (B) mark magnitude peaks arising from Fe−O bonds and edge- (e) and corner-sharing (c) Fe octahedra. In (B), dashed black lines plotted with spectra 2 and 3 show the Fh spectrum for reference.

During Fe(III) hydrolysis in the presence of 10 mol % dissolved P or Si relative to Fe, the poorly ordered FeOx that formed contained 9 mol % P (P9-FeOx$_{hydr}$) or Si (Si9-FeOx$_{hydr}$). The FeOx$_{hydr}$ with coprecipitated P and Si showed slightly less amplitude in the second and third peaks in the Fourier-transformed (FT) spectra ($R + \Delta R$ = 2.4 and 3.1 Å) that represent edge- and corner-sharing Fe octahedra. This may reflect inhibition of Fe polymerization and formation of aggregates of Fe oligomers linked by P or Si. This impact of strongly sorbing oxyanions such as phosphate, silicate, and arsenate on FeOx formation from Fe(III) hydrolysis has been described in detail in previous work.[6,9,10] The small decrease in peak amplitude under the current experimental conditions at P/Fe = 0.1 suggests that inhibition of Fe polymerization was minor under the current experimental conditions.

For Fe precipitates from Fe(II) oxidation, the impact of P or Si coprecipitation at an initial P/Fe ratio of 0.1 (10 mol % P relative to Fe) was more profound. In the absence of dissolved P or Si, pure Lp formed because freshly formed nanoscale FeOx undergoes rapid Fe(II)-catalyzed transformation.[23] The Lp showed a strongly developed second-shell Fe peak at ∼2.6 Å (uncorrected for phase shift) in the FT spectrum arising from edge-sharing Fe(III) octahedra (Figure 1B). The FT spectrum of P9-FeOx$_{oxid}$ (9 mol % P relative to Fe) was markedly different with decreased amplitudes of the Fe−O and edge-sharing Fe peaks. The P9-FeOx$_{oxid}$ spectrum represents a mixture of Fe phases, resulting from the sequential formation of Fe precipitates by Fe(II) oxidation in the presence of dissolved P.[7,8] Initially, highly disordered Fe(III)-P polymers and/or P-rich hydrous ferric oxide (P-HFO) form and rapidly deplete dissolved P. The Fe(III) that is subsequently formed under P-depleted conditions partly contributes to polymerization of Fe(III)-P into P-HFO and partly precipitates as Lp. Previous work indicates that under the current experimental conditions (P/Fe = 0.1), Fe precipitates most likely consist of a mixture of highly disordered P-HFO and Lp.[8] The LCF results showed that P9-FeOx$_{oxid}$ could be reproduced as a combination of P-HFO (70%) and Lp (30%). Assuming that all P was associated with the P-HFO fraction, this precipitate would have a molar P/Fe ratio of ∼0.13. The fraction of P-HFO was likely overestimated in the LFC procedure and therefore the P/Fe of the P-HFO would have been underestimated.

Dissolved Si has a lower affinity for Fe(III) and does not become depleted but rather coprecipitates with FeOx precipitates throughout FeOx synthesis, thereby shifting the reaction product of Fe(II) oxidation from Lp to Si-HFO.[3,7] Our results showed an Fe K-edge EXAFS spectrum of Si8-FeOx$_{oxid}$ (8 mol % Si relative to Fe) that was similar to that of pure Fh (Figure 1), with a more developed corner-sharing Fe peak compared to P9-FeOx$_{oxid}$ (Figure 1B). The PCA-ITFA results indicated that Si8-FeOx$_{oxid}$ consisted of 100% poorly ordered Si-HFO. The ITFA-LCF results are presented in detail in the Supporting Information.

Transformation of FeOx in Freshwater Sediment. The ITFA results for the entire Fe K-edge EXAFS data set indicated that all sample spectra, including starting materials, samples from freshwater Site 1, and samples from the sulfidation experiment, could be reproduced by three independent components that represented Fh, Lp, and FeS (see the Supporting Information).

The pore water in the freshwater drainage ditch was rich in Fe(II) (up to 600 μmol L^{-1}) and P (up to 566 μmol L^{-1}) (Figure 2A). Dissolved sulfide was not detected with the DGT sulfide-binding gel. Due to spectral similarity, all spectra of the hydrogel samples from Site 1 were reproduced in ITFA-LCF by one component: poorly ordered FeOx. To further explore potential minor changes in the FeOx structure, we also performed LCF on these samples in Athena[37] using Fh and P9-FeOx$_{hydr}$ or Si9-FeOx$_{hydr}$ as references. Preliminary LCF had shown that candidate references such as lepidocrocite, goethite, hematite, magnetite, vivianite, and siderite were all negligible. There were also no observable shifts in the Fe−K absorption edge (Figure 2B), further refuting the formation of reduced Fe phases in the hydrogels, even though chemical modeling in Visual Minteq 3.1 (settings: 500 μmol L^{-1} Fe(II) and P, pH 6.8, I = 0.01) indicated that the pore water was oversaturated (saturation index ≈ 8) with respect to vivianite. The LCF results indicated a shift from Si9-FeOx$_{hydr}$ and P9-FeOx$_{hydr}$ to Fh during deployment of the amended FeOx$_{hydr}$ (Figure 2B), suggesting a minor increase in the short-range structure. It is possible that aging during storage of the FeOx suspensions contributed to this change.

The limited extent of FeOx crystallization found here contrasts with the rapid and extensive Fe(II)-catalyzed transformation of poorly ordered FeOx observed in laboratory studies.[14,15,40−42] For example, Hansel et al.[15] observed that in sediment columns with advective flow of artificial groundwater with 100−300 μmol L^{-1} Fe(II), 70% of Fh was transformed into Lp and Gt within hours. Transformation will likely be more rapid under advective flow compared to our diffusion-limited experiment with passive samplers in natural sediment,

https://dx.doi.org/10.1021/acs.est.0c02352
Environ. Sci. Technol. 2020, 54, 12795−12802

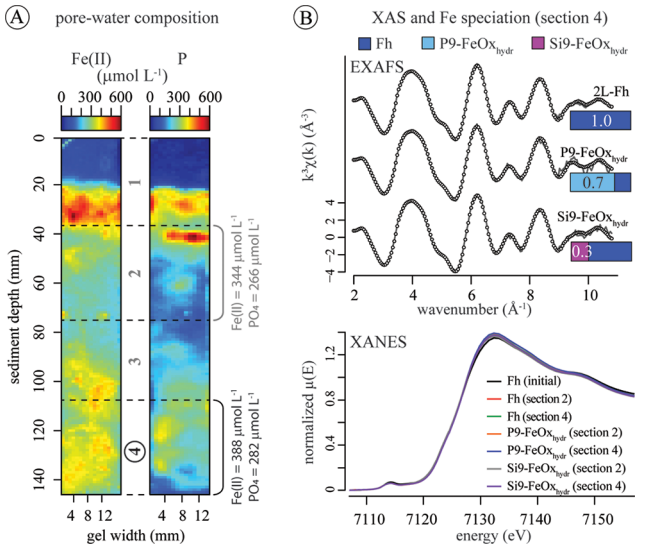

Figure 2. (A) Pore-water concentrations of Fe(II) and P in the freshwater sediment from Site 1. (B) Upper panel: data (lines) and fits (dots) for bulk Fe K-edge EXAFS spectra for selected FeOx-BT hydrogel sections after deployment (also see Figure S6 and Table S1). Bar charts show LCF results. Numbers in the bars show the fraction of the starting FeOx remaining. Lower panel: X-ray absorption near-edge spectroscopy (XANES) spectra of initial Fh and Fh, P9-FeOx$_{hydr}$, and Si9-FeOx$_{hydr}$ after deployment.

but significant FeOx transformation was expected during a four-week deployment in Fe(II)-rich sediment. Our observations are best explained by the difference in solution chemistry in the sediments relative to the aforementioned laboratory studies. The sediments we investigated were characterized by a high dissolved P concentration (>250 μmol L^{-1}) and are also likely to contain dissolved organic carbon. By binding to FeOx surfaces, P and other strongly sorbing inorganic and organic species can passivate the particle surface and decrease the rate of FeOx transformation.[4,6,43,44] However, we note that adsorbed species (P and organic carbon) were not determined in the current study.

Previous work showed that the apparently minor structural changes to Fh by coprecipitation of P or Si notably enhance reductive and acidic dissolution rates (i.e., destabilized the FeOx), likely due to altered macroscopic properties such as decreased particle aggregation.[2,6] In the current study, FeOx surface passivation by adsorption of P (and potentially other abundant pore-water species) overwhelmed any potential effects on altered FeOx properties from P or Si coprecipitation. Inhibition of FeOx transformation acts to preserve poorly ordered FeOx that have relatively high sorption capacity compared to more crystalline counterparts such as Lp and Gt.

In Situ Transformation of FeOx in Sulfidic Tidal Flat Sediment. The surface sediment from the tidal flat in the southwest of The Netherlands contained relatively low concentrations (<20 μmol L^{-1}) of dissolved Fe(II) and P compared to the freshwater ditch (see the Supporting Information) and showed signs of abundant burrows. During recovery of the samplers, we observed that sediment around the samplers had been eroded to different degrees, resulting in small-scale variability in the sediment depth interval covered by the sampler. Visual inspection of the FeOx-BT hydrogels after recovery showed strong variability in the depth of the sulfidation front, between 2 and 10 cm sediment depth (see the Supporting Information). Visual and spectroscopic evidence of FeOx transformation due to sulfidation was observed in all FeOx-BT hydrogels deployed at Site 2. However, the high spatial variability in chemical conditions in the sediment, likely due to tidal effects and bioturbation, did not allow for a systematic analysis of the effect of the FeOx structure on the degree of sulfidation. Therefore, in this section, we focus on individual samplers. The sharp transition from anoxic to sulfidic conditions with dissolved $\sum H_2S$ concentrations up to ~500 μmol L^{-1} as recorded by DGT sampling (which is an average calculated from integrated sulfide accumulation in the DGT gel over the deployment period[35]) (Figure 3A, left image) was reflected in an Lp-loaded hydrogel as a sharp color change (Figure 3A, right image). Synchrotron-based Fe speciation in the top and bottom slices of the Lp hydrogel showed complete transformation of Lp into iron monosulfide (FeS) during deployment in the sulfidic sediment (Figure 3B). The Fe K-edge XAS results did not show pyrite (FeS_2) formation in the analyzed gel sections from Site 2 after four weeks of deployment. These results highlight the potential for extensive alteration of gel-embedded FeOx. Furthermore, the results are in line with other field studies[39,45] that show relatively slow transformation of FeS to pyrite under natural sulfidic conditions compared to laboratory experiments.[46]

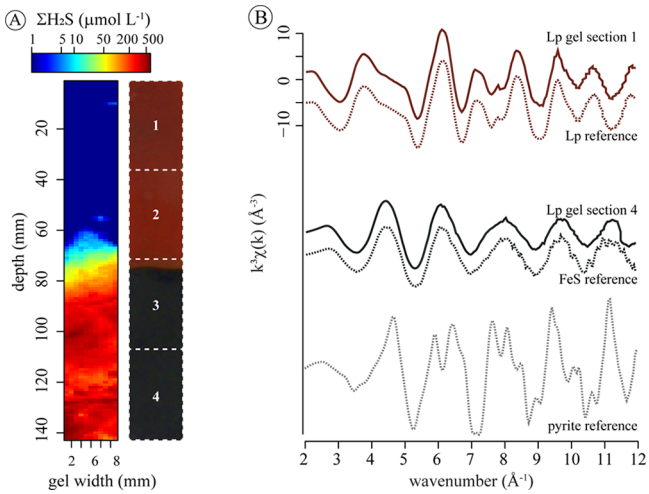

Figure 3. (A) Dissolved $\sum H_2S$ pore-water map determined by DGT hydrogel (left) and image of the Lp hydrogel (right) after four weeks of deployment in sediment with high dissolved $\sum H_2S$ at depth. Dashed lines and white numbers indicate sections into which the gel was cut for bulk Fe speciation. (B) Fe K-edge EXAFS spectra of Lp gel sections 1 and 4 plotted with the Lp, FeS, and pyrite (FeS_2) reference spectra.

To investigate the impact of reaction with dissolved sulfide on FeOx transformation and nutrient dynamics, high-resolution element scans were performed with μXRF on a P9-FeOx$_{hydr}$-loaded hydrogel. We selected intervals that captured the sulfidation front (S3, 7−10.5 cm) and a mottled sulfidation pattern (S4, 10.5−14 cm) (Figure 4). The μXRF line scan across the sulfidation front showed an increase in the solid-phase S content and a concurrent decrease in P (Figure 4A). A line scan across a patchy area in the bottom gel section (with better vacuum and higher counts) showed an even more clear anticorrelation between S and P (Figure 4B), reflecting the release of P by Fe sulfidation.[47] In contrast to S and P, Fe

https://dx.doi.org/10.1021/acs.est.0c02352
Environ. Sci. Technol. 2020, 54, 12795−12802

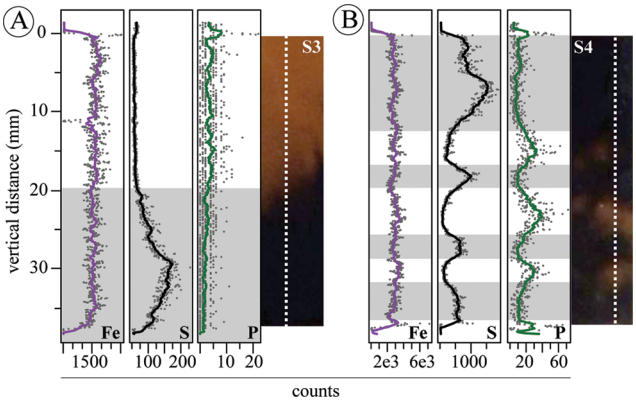

Figure 4. Micro-XRF line scans of iron (Fe), sulfur (S), and phosphorus (P) in sections of a P9-FeOx$_{hydr}$ hydrogel deployed under sulfidic field conditions at Site 2. Images of analyzed gel sections to the right, line scan indicated as dashed white line. (A) Scan across the sulfidation front. (B) Scan across the patchy region with sulfidized (dark) and non-sulfidized (light) areas.

counts were stable throughout the gel sections, irrespective of sulfidation. Similar stable Fe counts were observed across sulfidation fronts in hydrogels with Fh and Si9-FeOx$_{hydr}$ (data not shown). Leaching of Fe from FeOx-BT hydrogels was apparently limited during reaction with dissolved $\sum H_2S$, in line with sedimentary evidence for efficient Fe retention under sulfidic conditions.[48]

Laboratory-Based FeOx Sulfidation Experiment with Natural Sediment. Under stagnant conditions at room temperature (21 °C), dissolved $\sum H_2S$ accumulated with concentrations in excess of 2 mmol L^{-1} within 5 cm sediment depth (SI Section S2.6). Dissolved P showed an increase below ~1 cm sediment depth and reached concentrations at depths up to ~100 μmol L^{-1}. The DET for dissolved Fe(II) was compromised but indicated a similar small peak (<50 μmol L^{-1}) Fe(II) in the non-sulfidic surface sediment (0−2 cm sediment depth) as was observed in the sediment core (see the Supporting Information for details). We analyzed Fe speciation in mid-depth ($\sum H_2S$ 0.8−1.8 mmol L^{-1}) and bottom ($\sum H_2S$ ≥ 2 mmol L^{-1}) sections of FeOx-BT hydrogels after overnight deployment. The sample spectra and LCF results can be found in SI Section S2.7. The results showed that the degree of sulfidation (DOS, calculated here as FeS−Fe/Fe$_{tot}$) for FeOx from Fe(II) oxidation was consistently higher in bottom sections that were exposed to higher $\sum H_2S$ concentrations (Figure 5). For FeOx from Fe(III) hydrolysis, such a correlation between DOS and $\sum H_2S$ concentration was not observed.

When comparing the pure starting materials Fh and Lp, the DOS was higher for Lp (0.43−0.58) than for Fh (0.25). This may be attributed to the relatively rapid $\sum H_2S$ oxidation by Fh, leading to local depletion of $\sum H_2S$ and limited FeS formation. The reactivity of Lp toward sulfide is about an order of magnitude slower compared to Fh,[49,50] limiting $\sum H_2S$ depletion in and around the Lp-bearing hydrogel. Furthermore, laboratory studies on FeOx sulfidation pathways suggest that Fh-type FeOx can facilitate relatively rapid surface-to-bulk electron transport compared to more crystalline FeOx such as Lp. As a result, Fe(II) formed at the Fh surface by reaction with dissolved $\sum H_2S$ is re-oxidized to Fe(III) while structural non-sulfidized Fe(II) ("excess Fe(II)") forms, which prevents FeS formation at the Fh surface. This excess Fe(II) has been determined chemically but has so far escaped spectroscopic (Mössbauer) characterization.[18,51] In our study, ITFA-LCF did not indicate the presence of an Fe(II) phase other than FeS, but the Fe K-edge XANES data may provide some tentative evidence for the formation of non-sulfidized Fe(II) (see Supporting Information). Overall, diffusion-limited $\sum H_2S$ supply potentially combined with the formation of non-sulfidized excess Fe(II) at the expense of FeS formation may explain the relatively low DOS for poorly ordered Fh compared to Lp.

The DOS of P9-FeOx$_{hydr}$ and (to a lesser extent) Si9-FeOx$_{hydr}$ was elevated relative to pure Fh (Figure 5A). We propose that coprecipitation of P or Si lowers the rate of $\sum H_2S$ oxidation at the Fh surface (at P/Fe = 0.1, approximately half of the reactive surface sites on Fh-type FeOx are occupied[6,52]), thereby decreasing diffusion limitations to sulfidation as described above. Surface passivation by P has been suggested to inhibit the reaction of dissolved $\sum H_2S$ with FeOx surfaces.[44] Silicate sorption had a more limited effect on

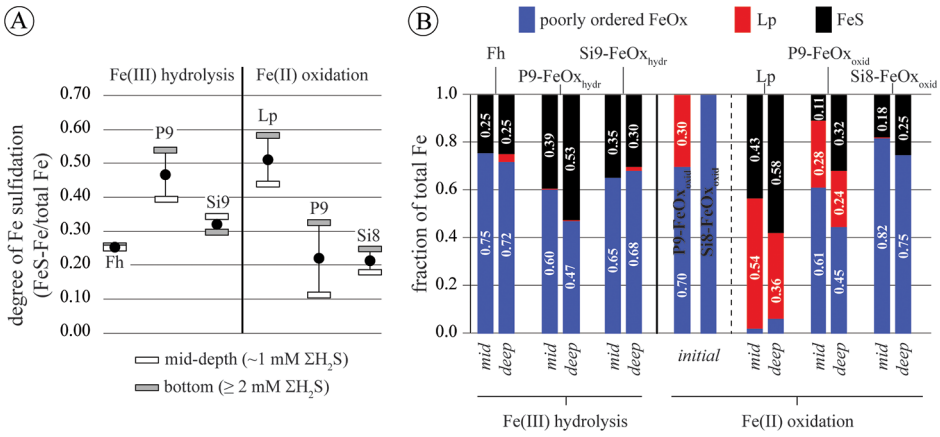

Figure 5. (A) Degree of Fe sulfidation (i.e., FeS as the fraction of total Fe) in FeOx-BT hydrogel sections, grouped by FeOx synthesis method (Fe(III) hydrolysis versus Fe(II) oxidation). White and gray bars represent DOS in mid-depth and bottom hydrogel sections, respectively; black dots indicate the mean DOS value (n = 2). (B) ITFA-LCF results for the FeOx-BT hydrogel sections. For reference, Fe speciation in the P9-FeOx$_{oxid}$ and Si8-FeOx$_{oxid}$ starting materials is shown. Mid and deep refer to mid-depth (3.5−7 cm) and bottom (10.5−14 cm) sections of the hydrogels, respectively.

https://dx.doi.org/10.1021/acs.est.0c02352
Environ. Sci. Technol. 2020, 54, 12795−12802

DOS than P, likely because Si has a lower affinity for FeOx surfaces.[7,53,54]

Coprecipitation of P or Si during Fe(II) oxidation resulted in a shift in reaction products from Lp to highly disordered HFO (Figure 1). Consistent with this shift to highly reactive FeOx that deplete dissolved $\sum H_2S$, the DOS of P9-FeOx$_{oxid}$ and Si8-FeOx$_{oxid}$ markedly decreased (0.1−0.3: Figure 5B) relative to Lp. For Si8-FeOx$_{oxid}$, the value and small range of DOS were similar to those of Fh, supporting the XAS results that indicated that Si8-FeOx$_{oxid}$ consisted of Si-HFO with a structure similar to that of Fh (Figures 1 and S3). Furthermore, the DOS of Si8-FeOx$_{oxid}$ indicated that occupation of FeOx surface sites by Si did not interfere with sulfidation under the experimental conditions ($\sum H_2S$ 1−2 mmol L^{-1}) and Si/Fe of ∼0.1. Moreover, the commonalities between Fh and Si8-FeOx$_{oxid}$ suggest that FeOx preparation by Fe(III) hydrolysis produces a poorly ordered FeOx that is representative of natural Fh-like material that commonly forms by Fe(II) oxidation in the presence of dissolved Si.[29]

For P9-FeOx$_{oxid}$, a 70:30 mixture of highly disordered P-HFO and Lp (Figures 1 and S3), the overall DOS showed relatively large variability (Figure 5B) and differences existed between DOS of the individual Fe components (Figure 5A). Approximately 5 and 20% of Lp was sulfidized in the mid-depth and bottom sections, respectively, compared to 10 and 40% for P-HFO. This suggests that reaction with highly reactive P-HFO can deplete $\sum H_2S$ and inhibit sulfidation of co-occurring Lp.

Implications. Our experimental approach with gel-based diffusive samplers was able to show that structural alterations in FeOx caused by coprecipitation of oxyanions such as PO_4 and SiO_4 can alter the environmental fate of FeOx. In the case of FeOx sulfidation, poorly ordered, highly reactive FeOx can rapidly deplete dissolved sulfide and thereby limit sulfidation and the associated release of nutrients and contaminants. Diffusion-limited resupply of dissolved sulfide may be more pronounced for gel-embedded FeOx but can also occur in natural sediments when local sulfide gradients develop due to the fast reaction of FeOx with sulfide. As such, differences in the rate and extent of sulfidation of FeOx might be particularly relevant in dynamic coastal systems with strong (diurnal) variations in redox conditions. At the same time, environmental conditions, such as high pore-water P concentrations and subsequent FeOx surface passivation, can be the dominating factor controlling FeOx transformations and overwhelm the effect of structural differences. Furthermore, our results show different behavior of amended FeOx from Fe(III) hydrolysis and Fe(II) oxidation, suggesting that laboratory-based findings from Fe(III)-derived Fh-type precipitates may not always be transferable to natural settings, where poorly ordered FeOx commonly form by Fe(II) oxidation. We show that deploying FeOx in natural sediments using gel-based diffusive samplers can elucidate the processes controlling environmental FeOx cycling under natural conditions and help bridge the gap between laboratory experiments and the environmental fate of FeOx.

■ ASSOCIATED CONTENT

Supporting Information

The Supporting Information is available free of charge at https://pubs.acs.org/doi/10.1021/acs.est.0c02352.

Detailed description of FeOx synthesis; preparation of hydrogels and samplers; deployment and recovery of samplers; analysis of DGT and DET gels; sample preparation and analysis for microscale XRF and XAS; PCA-ITFA results for the entire data set; ITFA-LCF results for P9-FeOx$_{oxid}$ and Si8-FeOx$_{oxid}$; Fe K-edge spectra and LCF results for FeOx deployed in freshwater Site 1; pore-water sulfide and phosphate for marine sediment in the laboratory microcosm experiment; results of ITFA analysis of the Fe K-edge EXAFS spectra for samples from the laboratory sulfidation experiment; and XANES results from the laboratory sulfidation experiment (PDF)

■ AUTHOR INFORMATION

Corresponding Author

Peter Kraal − *Department of Earth Sciences—Geochemistry, Faculty of Geosciences, Utrecht University, 3508 TA Utrecht, The Netherlands; NIOZ Royal Netherlands Institute for Sea Research, Department of Ocean Systems, 1790 AB Den Burg, The Netherlands;* orcid.org/0000-0002-6650-5680; Phone: +31-222-369455; Email: peter.kraal@nioz.nl

Authors

Case M. van Genuchten − *Department of Earth Sciences—Geochemistry, Faculty of Geosciences, Utrecht University, 3508 TA Utrecht, The Netherlands;* orcid.org/0000-0002-6697-0697

Wytze K. Lenstra − *Department of Earth Sciences—Geochemistry, Faculty of Geosciences, Utrecht University, 3508 TA Utrecht, The Netherlands*

Thilo Behrends − *Department of Earth Sciences—Geochemistry, Faculty of Geosciences, Utrecht University, 3508 TA Utrecht, The Netherlands;* orcid.org/0000-0002-0728-6545

Complete contact information is available at: https://pubs.acs.org/10.1021/acs.est.0c02352

Author Contributions

This manuscript was written through contributions of all authors. All authors have given approval to the final version of the manuscript.

Funding

This work was funded by a grant from the Dutch Research Council, NWO Veni grant 863.14.014, to P.K. This work was further supported by NWO DUBBLE grant 195.068.1039 for ESRF beamline BM26A.

Notes

The authors declare no competing financial interest.

■ ACKNOWLEDGMENTS

C.M.v.G. acknowledges NWO Veni grant 14400. W.K.L. acknowledges support through NWO-Vici Grant (865.13.005). The authors are grateful for the technical support and advice of Dipanjan Banerjee at the DUBBLE beamline during Fe K-edge EXAFS data collection. Anton Tramper, José Mogollón, Nikki Dijkstra, Simon Müller, and Silvia Hidalgo-Martinez assisted with field work in the Oosterschelde estuary. Simon Müller and Karel As kindly assisted with data collection at ESRF. The authors gratefully acknowledge the insightful and constructive feedback from three anonymous reviewers that greatly increased the quality of this article.

ABBREVIATIONS

DET	diffusive equilibrium in thin films
DGT	diffusive gradients in thin films
EXAFS	extended X-ray absorption fine structure
FeOx-BT	FeOx-bearing thin film
Fh	(2-line) ferrihydrite
Lp	lepidocrocite
XANES	X-ray absorption near-edge spectroscopy
XAS	X-ray absorption spectroscopy

REFERENCES

(1) van Genuchten, C. M.; Gadgil, A. J.; Peña, J. Fe(III) Nucleation in the Presence of Bivalent Cations and Oxyanions Leads to Subnanoscale 7 Å Polymers. *Environ. Sci. Technol.* **2014**, *48*, 11828−11836.

(2) Kaegi, R.; Voegelin, A.; Folini, D.; Hug, S. J. Effect of phosphate, silicate, and Ca on the morphology, structure and elemental composition of Fe(III)-precipitates formed in aerated Fe(II) and As(III) containing water. *Geochim. Cosmochim. Acta* **2010**, *74*, 5798−5816.

(3) Voegelin, A.; Kaegi, R.; Frommer, J.; Vantelon, D.; Hug, S. J. Effect of phosphate, silicate, and Ca on Fe(III)-precipitates formed in aerated Fe(II)- and As(III)-containing water studied by X-ray absorption spectroscopy. *Geochim. Cosmochim. Acta* **2010**, *74*, 164−186.

(4) Paige, C. R.; Snodgrass, W. J.; Nicholson, R. V.; Scharer, J. M.; He, Q. H. The effect of phosphate on the transformation of ferrihydrite into crystalline products in alkaline media. *Water, Air, Soil Pollut.* **1997**, *97*, 397−412.

(5) Cornell, R. M.; Giovanoli, R.; Schindler, P. W. Effect of silicate species on the transformation of ferrihydrite into goethite and hematite in alkaline media. *Clays Clay Miner.* **1987**, *35*, 21−28.

(6) Kraal, P.; van Genuchten, C. M.; Behrends, T.; Rose, A. L. Sorption of phosphate and silicate alters dissolution kinetics of poorly crystalline iron (oxyhydr)oxide. *Chemosphere* **2019**, *234*, 690−701.

(7) van Genuchten, C. M.; Peña, J.; Amrose, S. E.; Gadgil, A. J. Structure of Fe(III) precipitates generated by the electrolytic dissolution of Fe(0) in the presence of groundwater ions. *Geochim. Cosmochim. Acta* **2014**, *127*, 285−304.

(8) Voegelin, A.; Senn, A.-C.; Kaegi, R.; Hug, S. J.; Mangold, S. Dynamic Fe-precipitate formation induced by Fe(II) oxidation in aerated phosphate-containing water. *Geochim. Cosmochim. Acta* **2013**, *117*, 216−231.

(9) Waychunas, G. A.; Rea, B. A.; Fuller, C. C.; Davis, J. A. Surface chemistry of ferrihydrite: Part 1. EXAFS studies of the geometry of coprecipitated and adsorbed arsenate. *Geochim. Cosmochim. Acta* **1993**, *57*, 2251−2269.

(10) Rose, J.; Manceau, A.; Bottero, J.-Y.; Masion, A.; Garcia, F. Nucleation and growth mechanisms of Fe oxyhydroxide in the presence of PO_4 ions. 1. Fe K-Edge EXAFS study. *Langmuir* **1996**, *12*, 6701−6707.

(11) Rozan, T. F.; Taillefert, M.; Trouwborst, R. E.; Glazer, B. T.; Ma, S.; Herszage, J.; Valdes, L. M.; Price, K. S.; Iii, G. W. L. Iron-sulfur-phosphorus cycling in the sediments of a shallow coastal bay: Implications for sediment nutrient release and benthic macroalgal blooms. *Limnol. Oceanogr.* **2002**, *47*, 1346−1354.

(12) Krom, M. D.; Berner, R. A. Adsorption of phosphate in anoxic marine sediments. *Limnol. Oceanogr.* **1980**, *25*, 797−806.

(13) Cornell, R. M.; Schwertmann, U. *The Iron Oxides: Structure, Properties, Reactions, Occurrences and Uses*; Wiley, 2003; p 664.

(14) Hansel, C. M.; Benner, S. G.; Fendorf, S. Competing Fe(II)-induced mineralization pathways of ferrihydrite. *Environ. Sci. Technol.* **2005**, *39*, 7147−7153.

(15) Hansel, C. M.; Benner, S. G.; Neiss, J.; Dohnalkova, A.; Kukkadapu, R. K.; Fendorf, S. Secondary mineralization pathways induced by dissimilatory iron reduction of ferrihydrite under advective flow. *Geochim. Cosmochim. Acta* **2003**, *67*, 2977−2992.

(16) Burton, E. D.; Johnston, S. G.; Bush, R. T. Microbial sulfidogenesis in ferrihydrite-rich environments: Effects on iron mineralogy and arsenic mobility. *Geochim. Cosmochim. Acta* **2011**, *75*, 3072−3087.

(17) Yang, L.; Steefel, C. I.; Marcus, M. A.; Bargar, J. R. Kinetics of Fe(II)-Catalyzed Transformation of 6-line Ferrihydrite under Anaerobic Flow Conditions. *Environ. Sci. Technol.* **2010**, *44*, 5469−5475.

(18) Peiffer, S.; Behrends, T.; Hellige, K.; Larese-Casanova, P.; Wan, M.; Pollok, K. Pyrite formation and mineral transformation pathways upon sulfidation of ferric hydroxides depend on mineral type and sulfide concentration. *Chem. Geol.* **2015**, *400*, 44−55.

(19) Davison, W.; Zhang, H. In situ speciation measurements of trace components in natural waters using thin-film gels. *Nature* **1994**, *367*, 546−548.

(20) Davison, W.; Grime, G. W.; Morgan, J. A. W.; Clarke, K. Distribution of dissolved iron in sediment pore waters at submillimetre resolution. *Nature* **1991**, *352*, 323−325.

(21) Michel, F. M.; Ehm, L.; Antao, S. M.; Lee, P. L.; Chupas, P. J.; Liu, G.; Strongin, D. R.; Schoonen, M. A. A.; Phillips, B. L.; Parise, J. B. The structure of ferrihydrite, a nanocrystalline material. *Science* **2007**, *316*, 1726−1729.

(22) Hiemstra, T. Surface and mineral structure of ferrihydrite. *Geochim. Cosmochim. Acta* **2013**, *105*, 316−325.

(23) Schwertmann, U.; Cornell, S. *Iron Oxides in the Laboratory: Preparation and Characterization*; Wiley, 1991; p 188.

(24) Bigham, J. M.; Schwertmann, U.; Traina, S. J.; Winland, R. L.; Wolf, M. Schwertmannite and the chemical modeling of iron in acid sulfate waters. *Geochim. Cosmochim. Acta* **1996**, *60*, 2111−2121.

(25) Ferris, F. G.; Tazaki, K.; Fyfe, W. S. Iron oxides in acid mine drainage environments and their association with bacteria. *Chem. Geol.* **1989**, *74*, 321−330.

(26) Yu, J.-Y.; Heo, B.; Choi, I.-K.; Cho, J.-P.; Chang, H.-W. Apparent solubilities of schwertmannite and ferrihydrite in natural stream waters polluted by mine drainage. *Geochim. Cosmochim. Acta* **1999**, *63*, 3407−3416.

(27) Carlson, L.; Bigham, J. M.; Schwertmann, U.; Kyek, A.; Wagner, F. Scavenging of As from Acid Mine Drainage by Schwertmannite and Ferrihydrite: A Comparison with Synthetic Analogues. *Environ. Sci. Technol.* **2002**, *36*, 1712−1719.

(28) Jambor, J. L.; Dutrizac, J. E. Occurrence and constitution of natural and synthetic ferrihydrite, a widespread iron oxyhydroxide. *Chem. Rev.* **1998**, *98*, 2549−2586.

(29) Schwertmann, U. Occurrence and Formation of Iron Oxides in Various Pedoenvironments. In *Iron in Soils and Clay Minerals*; Stucki, J. W.; Goodman, B. A.; Schwertmann, U., Eds.; Springer Netherlands: Dordrecht, 1988; pp 267−308.

(30) Jensen, H. S.; Kristensen, P.; Jeppesen, E.; Skytthe, A. Iron-phosphorus ratio in surface sediment as an indicator of phosphate release from aerobic sediments in shallow lakes. *Hydrobiologia* **1992**, *235−236*, 731−743.

(31) Kraal, P.; Dijkstra, N.; Behrends, T.; Slomp, C. P. Phosphorus burial in sediments of the sulfidic deep Black Sea: key roles for adsorption by calcium carbonate and apatite authigenesis. *Geochim. Cosmochim. Acta* **2017**, *204*, 140−158.

(32) Hyacinthe, C.; Van Cappellen, P. An authigenic iron phosphate phase in estuarine sediments: composition, formation and chemical reactivity. *Mar. Chem.* **2004**, *91*, 227−251.

(33) Bennett, W. W.; Teasdale, P. R.; Welsh, D. T.; Panther, J. G.; Jolley, D. F. Optimization of colorimetric DET technique for the in situ, two-dimensional measurement of iron(II) distributions in sediment porewaters. *Talanta* **2012**, *88*, 490−495.

(34) Pagès, A.; Teasdale, P. R.; Robertson, D.; Bennett, W. W.; Schäfer, J.; Welsh, D. T. Representative measurement of two-dimensional reactive phosphate distributions and co-distributed iron(II) and sulfide in seagrass sediment porewaters. *Chemosphere* **2011**, *85*, 1256−1261.

(35) Robertson, D.; Teasdale, P. R.; Welsh, D. T. A novel gel-based technique for the high resolution, two-dimensional determination of

https://dx.doi.org/10.1021/acs.est.0c02352
Environ. Sci. Technol. 2020, 54, 12795−12802

iron (II) and sulfide in sediment. *Limnol. Oceanogr. Methods* **2008**, *6*, 502−512.
(36) Nikitenko, S.; Beale, A. M.; van der Eerden, A. M. J.; Jacques, S. D. M.; Leynaud, O.; O'Brien, M. G.; Detollenaere, D.; Kaptein, R.; Weckhuysen, B. M.; Bras, W. Implementation of a combined SAXS/WAXS/QEXAFS set-up for time-resolved in situ experiments. *J. Synchrotron Radiat.* **2008**, *15*, 632−640.
(37) Ravel, B.; Newville, M. Athena, Artemis, Hephaestus: data analysis for X-ray absorption spectroscopy using IFEFFIT. *J. Synchrotron Radiat.* **2005**, *12*, 537−541.
(38) Roßberg, A.; Reich, T.; Bernhard, G. Complexation of uranium(VI) with protocatechuic acid—application of iterative transformation factor analysis to EXAFS spectroscopy. *Anal. Bioanal. Chem.* **2003**, *376*, 631−638.
(39) Boesen, C.; Postma, D. Pyrite formation in anoxic environments of the Baltic. *Am. J. Sci.* **1988**, *288*, 575−603.
(40) Jones, A. M.; Collins, R. N.; Waite, T. D. Redox characterization of the Fe(II)-catalyzed transformation of ferrihydrite to goethite. *Geochim. Cosmochim. Acta* **2017**, *218*, 257−272.
(41) Pedersen, H. D.; Postma, D.; Jakobsen, R.; Larsen, O. Fast transformation of iron oxyhydroxides by the catalytic action of aqueous Fe(II). *Geochim. Cosmochim. Acta* **2005**, *69*, 3967−3977.
(42) Yee, N.; Shaw, S.; Benning, L. G.; Nguyen, T. H. The rate of ferrihydrite transformation to goethite via the Fe(II) pathway. *Am. Mineral.* **2006**, *91*, 92−96.
(43) Schoepfer, V. A.; Burton, E. D.; Johnston, S. G.; Kraal, P. Phosphate loading alters schwertmannite transformation rates and pathways during microbial reduction. *Sci. Total Environ.* **2019**, *657*, 770−780.
(44) Biber, M. V.; dos Santos Afonso, M.; Stumm, W. The coordination chemistry of weathering: IV. Inhibition of the dissolution of oxide minerals. *Geochim. Cosmochim. Acta* **1994**, *58*, 1999−2010.
(45) Kraal, P.; Burton, E. D.; Bush, R. T. Iron monosulfide accumulation and pyrite formation in eutrophic estuarine sediments. *Geochim. Cosmochim. Acta* **2013**, *122*, 75−88.
(46) Rickard, D. Kinetics of pyrite formation by the H_2S oxidation of iron (II) monosulfide in aqueous solutions between 25 and 125 °C: The rate equation. *Geochim. Cosmochim. Acta* **1997**, *61*, 115−134.
(47) Slomp, C. P.; Van Raaphorst, W. Phosphate adsorption in oxidized marine sediments. *Chem. Geol.* **1993**, *107*, 477−480.
(48) Scholz, F.; McManus, J.; Mix, A. C.; Hensen, C.; Schneider, R. R. The impact of ocean deoxygenation on iron release from continental margin sediments. *Nat. Geosci.* **2014**, *7*, 433−437.
(49) Poulton, S. W.; Krom, M. D.; Raiswell, R. A revised scheme for the reactivity of iron (oxyhydr)oxide minerals towards dissolved sulfide. *Geochim. Cosmochim. Acta* **2004**, *68*, 3703−3715.
(50) Canfield, D. E.; Raiswell, R.; Bottrell, S. H. The reactivity of sedimentary iron minerals toward sulfide. *Am. J. Sci.* **1992**, *292*, 659−683.
(51) Hellige, K.; Pollok, K.; Larese-Casanova, P.; Behrends, T.; Peiffer, S. Pathways of ferrous iron mineral formation upon sulfidation of lepidocrocite surfaces. *Geochim. Cosmochim. Acta* **2012**, *81*, 69−81.
(52) Dzombak, D. A.; Morel, F. M. M. *Surface Complexation Modeling: Hydrous Ferric Oxide*; Wiley: New York, 1990; p 416.
(53) Xu, N.; Christodoulatos, C.; Braida, W. Modeling the competitive effect of phosphate, sulfate, silicate, and tungstate anions on the adsorption of molybdate onto goethite. *Chemosphere* **2006**, *64*, 1325−1333.
(54) Hiemstra, T. Ferrihydrite interaction with silicate and competing oxyanions: Geometry and Hydrogen bonding of surface species. *Geochim. Cosmochim. Acta* **2018**, *238*, 453−476.

https://dx.doi.org/10.1021/acs.est.0c02352
Environ. Sci. Technol. 2020, 54, 12795−12802